Inorg. Chem. **2008**, *47*, 11920−11929

Straightforward Route to the Adamantane Clusters $[Sn_4Q_{10}]^{4-}$ (Q = S, Se, Te) and Use in the Assembly of Open-Framework Chalcogenides $(Me_4N)_2M[Sn_4Se_{10}]$ (M = Mn^{II}, Fe^{II}, Co^{II}, Zn^{II}) Including the First Telluride Member $(Me_4N)_2Mn[Ge_4Te_{10}]$

Konstantina Tsamourtzi,[†] Jung-Hwan Song,[‡] Thomas Bakas,[§] Arthur J. Freeman,[‡] Pantelis N. Trikalitis,*[,†] and Mercouri G. Kanatzidis*[,||]

Department of Chemistry, University of Crete, Voutes 71003, Heraklion, Greece, Department of Physics and Astronomy, Northwestern University, Evanston, Illinois 60208, Department of Physics, University of Ioannina, Ioannina 45110, Greece, and Department of Chemistry, Northwestern University, Evanston, Illinois 60208

Received September 13, 2008

The reaction of $K_2Sn_2Q_5$ (Q = S, Se, Te) with stoichiometric amounts of alkyl-ammonium bromides R_4NBr (R = methyl or ethyl) in ethylenediamine (*en*) afforded the corresponding salts $(R_4N)_4[Sn_4Q_{10}]$ (Q = S, Se, Te) in high yield. Although the compound $K_2Sn_2Te_5$ is not known, this reaction is also applicable to solids with a nominal composition "$K_2Sn_2Te_5$" which in the presence of R_4NBr in *en* are quantitatively converted to the salts $(R_4N)_4[Sn_4Te_{10}]$ on a multigram scale. These salts contain the molecular adamantane clusters $[Sn_4Q_{10}]^{4-}$ and can serve as soluble precursors in simple metathesis reactions with transition metal salts to synthesize the large family of open-framework compounds $(Me_4N)_2M[Sn_4Se_{10}]$ (M = Mn^{2+}, Fe^{2+}, Co^{2+}, Zn^{2+}). Full structural characterization of these materials as well as their magnetic and optical properties is reported. Depending on the transition metal in $(Me_4N)_2M[Sn_4Se_{10}]$, the energy band gaps of these compounds lie in the range of 1.27−2.23 eV. $(Me_4N)_2Mn[Ge_4Te_{10}]$ is the first telluride analogue to be reported in this family. This material is a narrow band gap semiconductor with an optical absorption energy of 0.69 eV. Ab initio electronic band structure calculations validate the semiconductor nature of these chalcogenides and indicate a nearly direct band gap.

Introduction

Open-framework metal sulfides,[1−16] selenides,[17−24] and tellurides[25,26] represent a growing class of multifunctional solids in which the various structural topologies and chemical compositions can be combined with porosity.[27] In these cases, the intrinsic chemical and physical properties associated with chalcogenides including optical, electronic, hydrophobic, and soft Lewis basic character could lead to unique behavior that cannot be achieved in other porous materials. For example, in a recent publication it was demonstrated that high surface area porous chalcogenide aerogels have a remarkable affinity and selectivity for Hg^{2+} cations and could be used in the removal of heavy metals from contaminated water.[28] In another example, crystalline microporous metal-chalcogenides have been shown to exhibit

* To whom correspondence should be addressed. E-mail: ptrikal@chemistry.uoc.gr (P.N.T.), m-kanatzidis@northwestern.edu (M.G.K.).
[†] University of Crete.
[‡] Department of Physics and Astronomy, Northwestern University.
[§] University of Ioannina.
[||] Department of Chemistry, Northwestern University.

(1) Wu, M.; Emge, T. J.; Huang, X. Y.; Li, J.; Zhang, Y. *J. Solid State Chem.* **2008**, *181*, 415–422.
(2) Manos, M. J.; Ding, N.; Kanatzidis, M. G. *Proc. Natl. Acad. Sci. U.S.A.* **2008**, *105*, 3696–3699.
(3) Zhang, Q. C.; Bu, X. H.; Han, L.; Feng, P. Y. *Inorg. Chem.* **2006**, *45*, 6684–6687.
(4) Ding, N.; Kanatzidis, M. G. *Chem. Mater.* **2007**, *19*, 3867–3869.
(5) Zheng, N. F.; Bu, X. H.; Feng, P. Y. *J. Am. Chem. Soc.* **2003**, *125*, 1138–1139.
(6) Bu, X. H.; Zheng, N. F.; Li, Y. Q.; Feng, P. Y. *J. Am. Chem. Soc.* **2003**, *125*, 6024–6025.
(7) Wang, C.; Li, Y. Q.; Bu, X. H.; Zheng, N. F.; Zivkovic, O.; Yang, C. S.; Feng, P. Y. *J. Am. Chem. Soc.* **2001**, *123*, 11506–11507.
(8) Wang, C.; Bu, X. H.; Zheng, N. F.; Feng, P. Y. *J. Am. Chem. Soc.* **2002**, *124*, 10268–10269.
(9) Austria, C.; Zhang, J.; Valle, H.; Zhang, Q. C.; Chew, E.; Nguyen, D. T.; Gu, J. Y.; Feng, P. Y.; Bu, X. H. *Inorg. Chem.* **2007**, *46*, 6283–6290.
(10) Cahill, C. L.; Parise, J. B. *J. Chem. Soc., Dalton Trans.* **2000**, *9*, 1475–1482.

10.1021/ic801762h CCC: $40.75
Published on Web 11/11/2008

fast-ion conductivity[29] with potential applications in areas such as batteries, fuel cells, electrochemical sensors, ion conducting membranes and photocatalysis.[30] In the majority of cases, hydro(solvo)thermal[30] synthesis has been the preferred tool of choice to discover open-framework chalcogenides partly because their crystal structures are hard to predict. However, the use of the tetrahedral $[MQ_4]^{4-}$,[31] dimeric $[M_2Q_6]^{4-}$, and the adamantane $[M_4Q_{10}]^{4-}$ anions as well defined chalcogenido building blocks in metathesis reactions with transition metal cations represents a more rational methodology that could lead to desired porous structures, as in the case of chalcogenide aerogels (chalcogels).[28] In order for this type of chemistry to advance at a more rapid pace, it is important to have these molecular precursors available in large quantities. Therefore, simple, general and convenient synthetic methodologies that allow the isolation of soluble precursors in high purity and yield are of great interest and, to the best of our knowledge, have not been reported.[32−37] We report here a straightforward method for the rapid, high yield, multigram scale synthesis of the salt precursors $(R_4N)_4[Sn_4Q_{10}]$, (R= methyl- or ethyl-; Q = S, Se, Te). To our best knowledge this is the first report on the synthesis of the adamantane tin sulfide anion $[Sn_4S_{10}]^{4-}$. Among the three tin chalcogenide $[Sn_4Q_{10}]^{4-}$ salts we found that only the selenides are completely soluble in water at room temperature. As a result, they react readily with transition metal cations to form the isostructural crystalline open-framework compounds $(Me_4N)_2M[Sn_4Se_{10}]$ ($M = Mn^{2+}$, Fe^{2+}, Co^{2+}, Zn^{2+}). These materials represent the heretofore "missing" heavier analogues of the germanium sulfide and selenide microporous family of solids that have been reported previously using the lighter adamantane anions $[Ge_4S_{10}]^{4-}$ [38−43] and $[Ge_4Se_{10}]^{4-}$,[44] respectively. The $(Me_4N)_2M[Sn_4Se_{10}]$ materials are semiconductors with a strong optical adsorption associated with band gap transition in the energy range 1.27−2.23 eV. The synthesis of the telluride analogues based on $[Sn_4Te_{10}]^{4-}$ or $[Ge_4Te_{10}]^{4-}$ (e.g., $(Me_4N)_2Mn[Ge_4Te_{10}]$) required a different methodology by directly reacting a "$K_2Ge_2Te_5$" alloy with $(Me_4N)Br$ and $MnCl_2 \cdot 4H_2O$ in H_2O. This material exhibits the most narrow energy band gap of this entire family with an absorption energy of 0.69 eV. Finally, for the first time, we report results of band structure calculations which shed light on the electronic structure of the open framework in this family of materials.

Experimental Section

Starting Materials. K_2Q (Q = S, Se, Te) were prepared in liquid ammonia using stoichiometric amounts of K and Q as described elsewhere.[45] All other chemicals were purchased from Aldrich and used as received.

$(R_4N)_4[Sn_4Q_{10}]$ (R = CH_3- or CH_3CH_2-; Q = S, Se, Te). All manipulations were carried out inside a nitrogen filled glovebox. First, solids with a chemical composition $K_2Sn_2Q_5$ were prepared by flame reaction in an evacuated quartz tube using stoichiometric amounts of K_2Q (5 mmol), Sn (10 mmol), and Q (20 mmol). The salts $(R_4N)_4[Sn_4Q_{10}]$ were synthesized in *en* (50 mL) at 100 °C by reacting stoichiometric amounts of $K_2Sn_2Q_5$ (5 mmol) and the corresponding tetraalkyl-ammomium bromides for 12 h. In all cases, the solid was isolated using suction filtration, washed with 50 mL of ethanol and dried under vacuum. The yield was >95% in all cases based on $K_2Sn_2Q_5$ (~3.8 g in the case of $(Me_4N)_4[Sn_4Se_{10}]$). Colors: $(Me_4N)_4[Sn_4S_{10}]$ light gray, $(R_4N)_4[Sn_4Se_{10}]$, yellow, and $(Et_4N)_4[Sn_4Te_{10}]$ black. This reaction is directly scaleable to much larger amounts as has been verified in the case of $(Me_4N)_4[Sn_4Se_{10}]$ by doubling the quantities of the starting materials $K_2Sn_2Se_5$ and Me_4NBr and obtaining ~8 g of the final product.

$(Me_4N)_2M[Sn_4Se_{10}]$ ($M = Mn^{2+}$, Fe^{2+}, Co^{2+}, Zn^{2+}). $(Me_4N)_4[Sn_4Se_{10}]$ (0.2 mmol) was dissolved in 10 mL of deionized water at room temperature forming a clear yellow solution. To this,

(11) Ahari, H.; Lough, A.; Petrov, S.; Ozin, G. A.; Bedard, R. L. *J. Mater. Chem.* **1999**, *9*, 1263–1274.
(12) Ahari, H.; Dag, O.; Petrov, S.; Ozin, G. A.; Bedard, R. L. *J. Phys. Chem. B* **1998**, *102*, 2356–2366.
(13) Ahari, H.; Bowes, C. L.; Jiang, T.; Lough, A.; Ozin, G. A.; Bedard, F. L.; Petrov, S.; Young, D. *Adv. Mater.* **1995**, *7*, 375–378.
(14) Li, H. L.; Kim, J.; O'Keeffe, M.; Yaghi, O. M. *Angew. Chem., Int. Ed.* **2003**, *42*, 1819–1821.
(15) Li, H. L.; Kim, J.; Groy, T. L.; O'Keeffe, M.; Yaghi, O. M. *J. Am. Chem. Soc.* **2001**, *123*, 4867–4868.
(16) Li, H. L.; Laine, A.; O'Keeffe, M.; Yaghi, O. M. *Science* **1999**, *283*, 1145–1147.
(17) Manos, M. J.; Jang, J. I.; Ketterson, J. B.; Kanatzidis, M. G. *Chem. Commun.* **2008**, 972–974.
(18) Bu, X. H.; Zheng, N. F.; Wang, X. Q.; Wang, B.; Feng, P. Y. *Angew. Chem., Int. Ed.* **2004**, *43*, 1502–1505.
(19) Wang, C.; Bu, X. H.; Zheng, N. F.; Feng, P. Y. *Chem. Commun.* **2002**, 1344–1345.
(20) Manos, M. J.; Malliakas, C. D.; Kanatzidis, M. G. *Chem.-Eur. J.* **2007**, *13*, 51–58.
(21) Dehnen, S.; Melullis, M. *Coord. Chem. Rev.* **2007**, *251*, 1259–1280.
(22) Wu, M.; Sul, W. P.; Jasutkar, N.; Huang, X. Y.; Li, J. *Mater. Res. Bull.* **2005**, *40*, 21–27.
(23) Dhingra, S.; Kanatzidis, M. G. *Science* **1992**, *258*, 1769–1772.
(24) Vaqueiro, P. *Inorg. Chem.* **2008**, *47*, 20–22.
(25) Wang, C.; Bu, X. H.; Zheng, N. F.; Feng, P. Y. *Angew. Chem., Int. Ed.* **2002**, *41*, 1959–1961.
(26) Ruzin, E.; Dehnen, S. *Z. Anorg. Allg. Chem.* **2006**, *632*, 749–755.
(27) Zheng, N. F.; Bu, X. G.; Wang, B.; Feng, P. Y. *Science* **2002**, *298*, 2366–2369.
(28) Bag, S.; Trikalitis, P. N.; Chupas, P. J.; Armatas, G. S.; Kanatzidis, M. G. *Science* **2007**, *317*, 490–493.
(29) Zheng, N. F.; Bu, X. H.; Feng, P. Y. *Nature* **2003**, *426*, 428–432.
(30) Feng, P. Y.; Bu, X. H.; Zheng, N. F. *Acc. Chem. Res.* **2005**, *38*, 293–303.
(31) Parise, J. B.; Corbin, D. R.; Abrams, L.; Northrup, P.; Rakovan, J.; Nenoff, T. M.; Stucky, G. D. *Zeolites* **1994**, *14*, 25–34.
(32) Fehlker, A.; Blachnik, R. *Z. Anorg. Allg. Chem.* **2001**, *627*, 1128–1134.
(33) Fehlker, A.; Blachnik, R. *Z. Anorg. Allg. Chem.* **2001**, *627*, 411–418.
(34) Park, C.-W.; Pell, M. A.; Ibers, J. A. *Inorg. Chem.* **1996**, *35*, 4555–4558.
(35) Pirani, A. M.; Mercier, H. P. A.; Dixon, D. A.; Borrmann, H.; Schrobilgen, G. J. *Inorg. Chem.* **2001**, *40*, 4823–4829.
(36) Campbell, J.; Diciommo, D. P.; Mercier, H. P. A.; Pirani, A. M.; Schrobilgen, G. J.; Willuhn, M. *Inorg. Chem.* **1995**, *34*, 6265–6272.
(37) Sheldrick, W. S.; Schaaf, B. *Z. Naturforsch. B* **1994**, *49*, 655–659.
(38) Bedard, R. L.; Wilson, S. T.; Vail, L. D.; Bennett, J. M.; Flanigen, E. M. In *Zeolites: Facts, Figures, Future. Proceedings of the 8th International Zeolite Conference*; Jacobs, P. A., van Santen, R. A., Eds.; Elsevier: Amsterdam, 1989, pp 375−387.
(39) Yaghi, O. M.; Sun, Z.; Richardson, D. A.; Groy, T. L. *J. Am. Chem. Soc.* **1994**, *116*, 807–808.
(40) Bowes, C. L.; Huynh, W. U.; Kirkby, S. J.; Malek, A.; Ozin, G. A.; Petrov, S.; Twardowski, M.; Young, D.; Bedard, R. L.; Broach, R. *Chem. Mater.* **1996**, *8*, 2147–2152.
(41) Bowes, C. L.; Lough, A. J.; Malek, A.; Ozin, G. A.; Petrov, S.; Young, D. *Chem. Ber.* **1996**, *129*, 283–287.
(42) Cahill, C. L.; Ko, Y. H.; Hanson, J. C.; Tan, K. M.; Parise, J. B. *Chem. Mater.* **1998**, *10*, 1453–1458.
(43) Achak, O.; Pivan, J. Y.; Maunaye, M.; Louer, M.; Louer, D. *J. Solid State Chem.* **1996**, *121*, 473–478.
(44) Ahari, H.; Garcia, A.; Kirkby, S.; Ozin, G. A.; Young, D.; Lough, A. J. *J. Chem. Soc., Dalton Trans.* **1998**, 2023–2027.
(45) Axtell, E. A.; Park, Y.; Chondroudis, K.; Kanatzidis, M. G. *J. Am. Chem. Soc.* **1998**, *120*, 124–136.

Scheme 1. Three-Dimensional Sn−Se Covalent Network in $K_2Sn_2Se_5$ (left) When Treated with Small Alkyl-Ammonium Bromides in *en* is Transformed into Molecular Adamantane $[Sn_4Se_{10}]^{4-}$ Clusters (right)

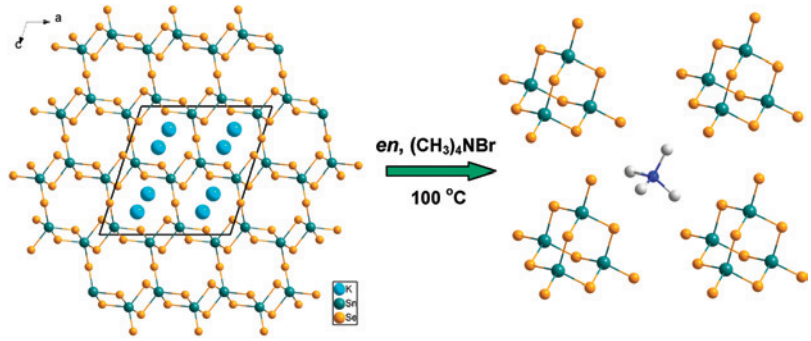

$MnCl_2 \cdot 4H_2O$ (0.2 mmol) dissolved in 5 mL of H_2O added slowly over a period of 2 min using a pipet. A red microcrystalline solid was immediately formed which was isolated by suction filtration, washed with 10 mL of H_2O and dried under vacuum. The yield was >80% based on $(Me_4N)_4[Sn_4Se_{10}]$. The isostructural compounds of iron (black) and cobalt (orange) were synthesized using $FeCl_2 \cdot 4H_2O$ and $CoCl_2 \cdot 4H_2O$ respectively, following exactly the same procedure. In the case of zinc, the isostructural crystalline product (yellow) was obtained when the solution of $ZnCl_2 \cdot 4H_2O$ (0.2 mmol) was combined with Na_4EDTA (EDTA: ethylenediamine-tetraacetate) in an equimolar amount.

$(Me_4N)_2Mn[Ge_4Te_{10}]$. A solid with a nominal chemical composition "$K_2Ge_2Te_5$" was prepared in an evacuated quartz tube by combining stoichiometric amounts of K_2Te (0.3 mmol), Ge (0.6 mmol), and Te (1.2 mmol) and melting the mixture to a free flowing melt using a direct flame. A mixture of $K_2Ge_2Te_5$ (0.5 mmol), $MnCl_2 \cdot 4H_2O$ (0.25 mmol), and $(Me_4N)Br$ (0.5 mmol) in 50 mL of *en* was reacted at 100 °C for 12 h. A black solid was isolated by suction filtration, washed with 10 mL of MeOH, and dried under vacuum. A yield of >80% based on $K_2Ge_2Te_5$ was obtained.

Physical Measurements. Single crystal data were collected at room temperature on a Siemens Platform SMART CCD diffractometer using Mo Kα radiation (λ = 0.71073 Å). An empirical absorption correction was done using SADABS, and the full anisotropic structure refinement was carried out using the SHELXTL programs. Powder X-ray diffraction data (XRD) were collected on a Rigaku D/MAX-2000H rotating anode diffractometer (Cu Kα radiation) equipped with a secondary pyrolytic graphite monochromator operated at 40 kV and 178 mA. The scan rates were between 0.10 and 0.15 deg/min with a step size of 0.01 deg. Powder XRD pattern indexing and lattice parameters refinement were performed using the software WinPLOTR of the FullProf Suite for Windows.[61] Bulk DC magnetic susceptibility measurements were carried out with a commercial Maglab Exa Oxford instrument. Zero field-cooled runs were performed between 5 K and room temperature and a magnetic field of 0.5 T. Scanning electron microscope (SEM) images were collected on a JEOL JSM-6400V instrument. ^{119}Sn and ^{57}Fe Mössbauer spectra were obtained with a constant acceleration spectrometer using a 5mCi $CaSnO_3$ and ^{57}Co (Rh) sources, respectively (sources kept at room temperature). The corresponding isomer shift values are reported relative to $CaSnO_3$ and α-Fe.

Thermogravimetric analyses (TGA) were performed using a TA SDT Q-600 analysis system. Typically, 20 mg of sample was placed in an alumina bucket and heated in a nitrogen flow of 50 mL/min with a rate of 10 °C/min.

Infrared spectra (IR) in the mid-IR (4000−600 cm^{-1}, KBr pellet) and far-IR region (600−100 cm^{-1}, CsI pellet) were recorded with a computer-controlled Nicolet 750 Magna-IR series II spectrometer equipped with a TGS/PE detector and silicon beam splitter in 2-cm^{-1} resolution. Raman spectra were recorded on a Holoprobe Raman spectrograph equipped with a 633 nm HeNe laser and a CCD camera detector. The instrument was coupled to an Olympus BX60 microscope. Crystals or powder were simply placed onto a small glass slide, and a 10× objective lens was used to choose the area of the specimens to be measured.

UV−vis/near-IR diffuse reflectance spectra were obtained at room temperature on a Shimadzu UV-3101PC double-beam, double monochromator spectrophotometer in the wavelength range of 200−2500 nm. $BaSO_4$ powder was used as a reference (100% reflectance) and base material on which the powder sample was coated. Reflectance data were converted to absorbance data as described elsewhere.[46]

Results and Discussion

Synthesis and X-ray Diffraction Studies. In our initial attempt to synthesize the potassium salt of the adamantane anions $[Sn_4Se_{10}]^{4-}$ we reacted stoichiometric amounts of K_2Se, Sn, and Se in an evacuated quartz tube using a flame. A well flowing melt was formed within a few minutes which upon cooling gave a crystalline product in the form of an ingot. Glass attack by the melt was not observed, and the product was found to be relatively air stable. X-ray powder diffraction analysis revealed that the product was pure $K_2Sn_2Se_5$, a known three-dimensional selenostannate compound.[47] Interestingly, we found that when this material is treated with solution of $(Me_4N)Br$ or $(Et_4N)Br$ in *en*, it undergoes ion-exchange and structurally rearranges to give pure $(R_4N)_4[Sn_4Se_{10}]$ solids according to the reaction:

$$2K_2Sn_2Se_5 + 4(R_4N)Br \rightarrow (R_4N)_4[Sn_4Se_{10}] + 4KBr \quad (1)$$

This ion-exchange induced chemical and structural transformation is shown in Scheme 1. A similar methodology has been reported for the synthesis of $(Et_4N)_4[Ge_4Te_{10}]$[48] but not for any other Group 14 chalcogeno-metalate adamantane anions. As shown in Figure 1, the powder XRD pattern of $(Et_4N)_4[Sn_4Se_{10}]$ matches very well with that calculated from the single crystal data[49] of the same compound synthesized electrochemically, indicating the formation of a pure product.

(46) McCarthy, T. J.; Ngeyi, S. P.; Liao, J. H.; Degroot, D. C.; Hogan, T.; Kannewurf, C. R.; Kanatzidis, M. G. *Chem. Mater.* **1993**, *5*, 331–340.
(47) Klepp, K. O. *Z. Naturforsch., B* **1992**, *47*, 197–200.
(48) Dhingra, S. S.; Haushalter, R. C. *Polyhedron* **1994**, *13*, 2775–2779.
(49) Park, C. W.; Pell, M. A.; Ibers, J. A. *Inorg. Chem.* **1996**, *35*, 4555–4558.

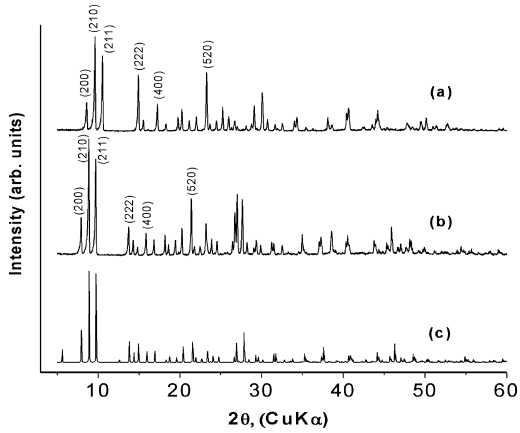

Figure 1. Powder X-ray diffraction patterns for (a) $(Me_4N)_4[Sn_4Se_{10}]$ and (b) $(Et_4N)_4[Sn_4Se_{10}]$ (c) calculated pattern from the crystal structure of $(Et_4N)_4[Sn_4Se_{10}]$.

Table 1. Refined Lattice Parameters of the Chalcogenostannate Adamantane Salts

compound	lattice type	lattice constant (Å)
$(Me_4N)_4[Sn_4S_{10}]$	primitive cubic $P\bar{4}3n$	19.975(8)
$(Me_4N)_4[Sn_4Se_{10}]$	primitive cubic $P\bar{4}3n$	20.568(8)
$(Et_4N)_4[Sn_4Se_{10}]$	primitive cubic $P\bar{4}3n$	22.316(4)
$(Et_4N)_4[Sn_4Te_{10}]$	primitive cubic $P\bar{4}3n$	23.098(8)

This material crystallizes in the primitive cubic space group $P\bar{4}3n$. Consistent with the formation of an isostructural compound, $(Me_4N)_4[Sn_4Se_{10}]$ shows a very similar powder XRD pattern but shifted to higher Bragg angles as expected from the smaller size of the Me_4N^+ counterions. The lattice parameters of these materials are given in Table 1.

The above synthetic method was found to be very general, and according to reaction 1 we have synthesized the sulfostannate $[Sn_4S_{10}]^{4-}$ and tellurostannate $[Sn_4Te_{10}]^{4-}$ adamantane anions starting from $K_2Sn_2S_5$ and $K_2Sn_2Te_5$ solids, respectively. We note that $K_2Sn_2S_5$ is a crystalline three-dimensional solid isostructural to the selenide analogue;[47] however, the solid with a chemical composition $K_2Sn_2Te_5$ is an amorphous phase. The powder XRD patterns of the compounds $(Me_4N)_4[Sn_4S_{10}]$ and $(Et_4N)_4[Sn_4Te_{10}]$ are shown in Figure 2, which can be indexed in a primitive cubic lattice and are isostructural to the corresponding selenostannate salts. Their lattice parameters are given in Table 1. It is important to note that the isolation of the adamantane $[Sn_4S_{10}]^{4-}$ anion is reported here for the first time. The crystal structure of the tellurostannate $[Sn_4Te_{10}]^{4-}$ anion has been reported previously; however, it has been isolated in very low yield as a crown ether potassium salt following a complicated extraction procedure.[35]

Our methodology is also suitable for the synthesis of $[Ge_4S_{10}]^{4-}$ and $[Ge_4Se_{10}]^{4-}$ adamantane anions with several small tetra-alkyl-ammonium counterions (data not shown); however, we were not able to isolate the tellurogermanate $[Ge_4Te_{10}]^{4-}$ analogue.

The availability of the $[Sn_4Q_{10}]^{4-}$ anions in high yield allowed us to examine their use as building blocks for the construction of open-framework materials. In particular, we

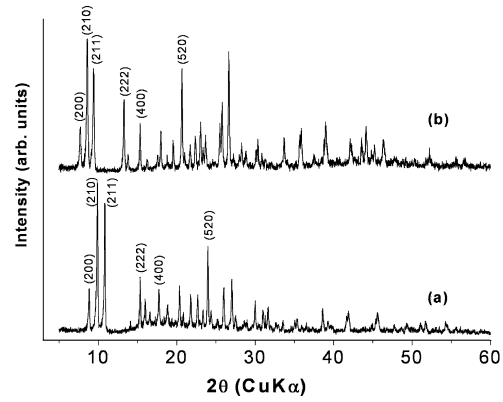

Figure 2. Powder X-ray diffraction patterns for (a) $(Me_4N)_4[Sn_4S_{10}]$ and (b) $(Et_4N)_4[Sn_4Te_{10}]$.

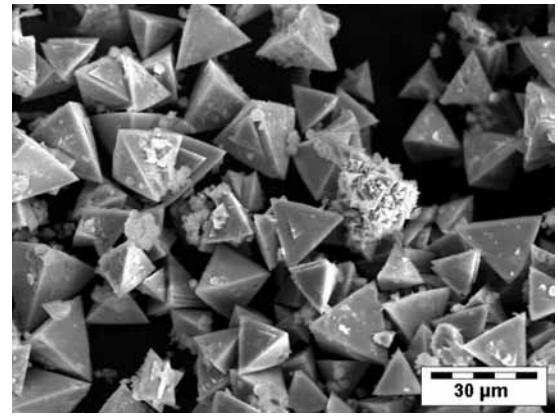

Figure 3. Scanning electron micrograph image of typical crystals of $(Me_4N)_2Fe[Sn_4Se_{10}]$ with pseudotetrahedral morphology.

investigated whether these anions could be combined with transition metals in solution to form extended solids via metathesis reactions, as has been reported for the lighter chalcogenogermanate $[Ge_4Q_{10}]^{4-}$ anions.[39,41−44] We examined first the stability of these anions in aqueous solutions and found that only the $(R_4N)_4[Sn_4Se_{10}]$ salts are readily soluble forming pale-yellow solutions. The sulfide analogue $(Me_4N)_4[Sn_4S_{10}]$ decomposes in H_2O forming the layered compound $(Me_4N)_2Sn_3S_7$.[50] In the case of $[Sn_4Te_{10}]^{4-}$, an amorphous phase was obtained.

The reaction of $[Sn_4Se_{10}]^{4-}$ anions with divalent first-row transition metal cations in aqueous solution at room temperature resulted in the formation of crystalline materials, according to the following chemical equation:

$$(Me_4N)_4[Sn_4Se_{10}] + MCl_2 \rightarrow (Me_4N)_2M[Sn_4Se_{10}] + 2(Me_4N)Cl, \quad M = Mn^{2+}, Fe^{2+}, Co^{2+}, Zn^{2+} \quad (2)$$

The metathesis reaction 2 is instantaneous, and in the case of cobalt and zinc only microcrystalline powders were obtained. In contrast, when manganese and iron were employed as linking cations, small crystals with pseudotetrahedral morphology were obtained, as shown in Figure 3. Slightly larger single crystals suitable for X-ray diffraction analysis were isolated from the manganese sample. The corresponding crystallographic analysis results are summarized in Table 2. Selected bond lengths and bond angles are shown in Tables 3 and 4, respectively. The compound

(50) Parise, J. B.; Ko, Y. H.; Rijssenbeek, J.; Nellis, D. M.; Tan, K. M.; Koch, S. *J. Chem. Soc.-Chem. Commun.* **1994**, 527–527.

Table 2. Crystal Data and Structure Refinement for $(Me_4N)_2Mn[Sn_4Se_{10}]$

empirical formula	$C_8N_2H_{24}MnSn_4Se_{10}$
formula weight	1467.59
temperature	297(2) K
wavelength	0.71073 Å
crystal system, space group	tetragonal, $I\bar{4}$
unit cell dimensions	$a = 9.932(2)$ Å
	$b = 9.932(2)$ Å
	$c = 15.374(3)$ Å
volume	1516.6(4) Å^3
Z, calculated density	2, 3.214 Mg/m^3
absorption coefficient	15.655 mm^{-1}
$F(000)$	1302
crystal size	0.04 × 0.04 × 0.04 mm
theta range for data collection	2.44−26.00 deg
limiting indices	$-12 \le h \le 6$, $-12 \le k \le 10$, $-18 \le l \le 18$
reflections collected/unique	3878/1503 [R(int) = 0.0829]
completeness to theta = 26.00	100.0%
refinement method	full-matrix least-squares on F^2
data/restraints/parameters	1503/0/61
goodness-of-fit on F^2	0.987
final R indices [$I > 2\sigma(I)$][a]	$R_1 = 0.0535$, $wR_2 = 0.0810$
R indices (all data)[a]	$R_1 = 0.0845$, $wR_2 = 0.0926$
absolute structure parameter	0.11(3)
extinction coefficient	0.00027(7)
largest diff. peak and hole	0.812 and −0.893 e·Å^{-3}

[a] $R_1 = \sum||F_o| - |F_c||/\sum|F_o|$, $wR_2 = [\sum w(F_o^2 - F_c^2)^2/\sum w(F_o^2)^2]^{1/2}$.

Table 3. Atomic Coordinates (×10^4) and Equivalent Isotropic Displacement Parameters (Å^2 × 10^3) for $(Me_4N)_2Mn[Sn_4Se_{10}]$

	x	y	z	U(eq)[a]
Sn	4199(1)	8138(1)	8427(1)	26(1)
Se(1)	5000	10000	9438(1)	38(1)
Se(2)	2239(2)	8882(2)	7476(1)	38(1)
Se(3)	3117(2)	6341(2)	9271(1)	39(1)
Mn	5000	5000	10000	26(1)
N(1)	10000	5000	7500	29(6)
C(1)	8808(14)	4623(16)	6944(9)	39(4)
N(2)	5000	5000	5000	37(7)
C(2)	6080(20)	4400(20)	5547(13)	90(7)

[a] U(eq) is defined as one-third of the trace of the orthogonalized U_{ij} tensor.

crystallizes in the tetragonal space group $I\bar{4}$ with chemical formula $(Me_4N)_2Mn[Sn_4Se_{10}]$, isostructural to $(Me_4N)_2Mn[Ge_4Q_{10}]$ (Q = S, Se).[39,44]

As shown in Figure 4, the anionic framework $^3_\infty[MnSn_4Se_{10}]^{2-}$ is made up of tetrahedral Mn^{2+} cations, where each cation is covalently linked into a three-dimensional arrangement to four terminal selenide atoms from four different adamantane $[Sn_4Se_{10}]^{4-}$ units. Microporous tunnels of approximately 5 × 8 Å in size are formed and run along the [100] and [010] crystallographic directions inside of which Me_4N^+ counterions are located. This is a zinc-blende open framework-type structure in which all tetrahedral sites are alternately substituted by $[Sn_4Se_{10}]^{4-}$ clusters and pseudotetrahedral $MnSe_4$ units. The Sn−Se_b bond distances range from 2.5217(19) Å to 2.5444(19) Å. The Sn−Se_t distance is 2.4538(19) Å; the Sn−Se−Sn bond angles are between 100.38(6)−112.28(6)°. These values agree with those observed in the crystal structure of $(Et_4N)_4[Sn_4Se_{10}]$,[49] [2,2,2-Crypt-K]$_4[Sn_4Se_{10}]$,[36] and $[(C_4H_9)_2NH_2]_4[Sn_4Se_{10}]$[51] indicating no considerable structural changes of the adamantane clusters in the framework.

(51) Fehlker, A.; Blachnik, R. *Z. Anorg. Allg. Chem.* **2001**, *627*, 411–418.

Table 4. Selected Bond Lengths (Å) and Angles (deg) for $(Me_4N)_2Mn[Sn_4Se_{10}]$[a]

Sn−Se(3)	2.453(9)
Sn−Se(2)^1	2.521(8)
Sn−Se(1)	2.543(6)
Sn−Se(2)	2.544(5)
Se(1)-Sn^2	2.543(6)
Se(2)-Sn^3	2.521(8))
Mn−Se(3)^4	2.554(8)
Mn−Se(3)	2.554(8)
Mn−Se(3)^5	2.554(8))
Mn−Se(3)^6	2.554(8)
Se(3)−Sn−Se(2)^1	111.38(7)
Se(3)−Sn−Se(1)	110.05(7)
Se(2)^1−Sn−Se(1)	110.95(6)
Se(3)−Sn−Se(2)	100.38(6)
Se(2)^1−Sn−Se(2)	111.38(4)
Se(1)−Sn−Se(2)	112.28(6)
Sn−Se(1)−Sn^2	104.67(8)
Sn^3−Se(2)−Sn	105.38(7)
Se(3)^4−Mn−Se(3)	101.09(3)
Se(3)^4−Mn−Se(3)^6	101.09(3)
Se(3)^4−Mn−Se(3)^5	127.96(8)
Se(3)−Mn−Se(3)^5	127.96(8)
Se(3)−Mn−Se(3)^6	101.09(3)
Se(3)^5−Mn−Se(3)^6	101.09(3)

[a] Symmetry transformations used to generate equivalent atoms: (1) $-y + 3/2, x + 1/2, -z + 3/2$; (2) $-x + 1, -y + 2, z$; (3) $y - 1/2, -x + 3/2, -z + 3/2$; (4) $y, -x + 1, -z + 2$; (5) $-x + 1, -y + 1, z$; (6) $-y + 1, x, -z + 2$; (7) $-x + 2, -y + 1, z$; (8) $y + 1/2, -x + 3/2, -z + 3/2$; (9) $-y + 3/2, x - 1/2, -z + 3/2$; (10) $-y + 1, x, -z + 1$; (11) $y, -x + 1, -z + 1$.

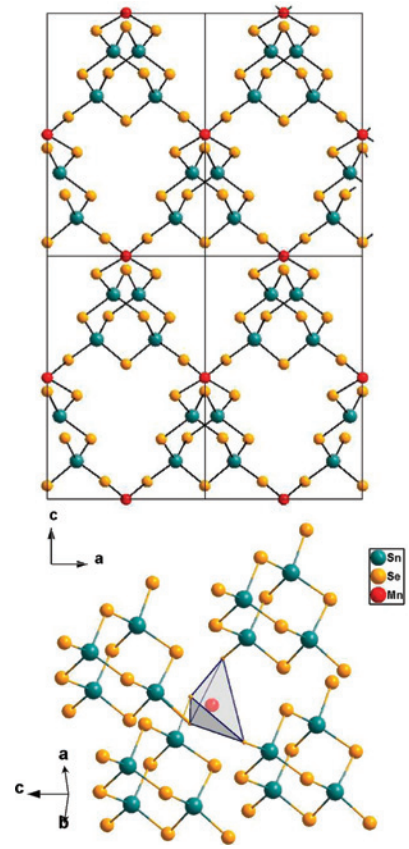

Figure 4. 2 × 2 × 2 representation of the tetragonal structure $(Me_4N)_2Mn[Sn_4Se_{10}]$ looking down the [010] crystallographic axis (top) and the distorted Mn(II) tetrahedral sites linking four independent adamantane $[Sn_4Se_{10}]^{4-}$ building units (bottom). The Me_4N^+ counterions are omitted for clarity.

The $MnSe_4$ tetrahedral building units are highly distorted in which two Se−Mn−Se bond angles are 127.96(8)° and four

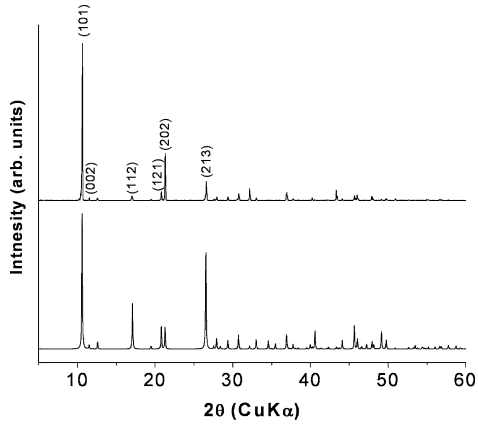

Figure 5. Experimental and simulated (bottom) powder X-ray diffraction patterns (top) for $(Me_4N)_2Mn[Sn_4Se_{10}]$.

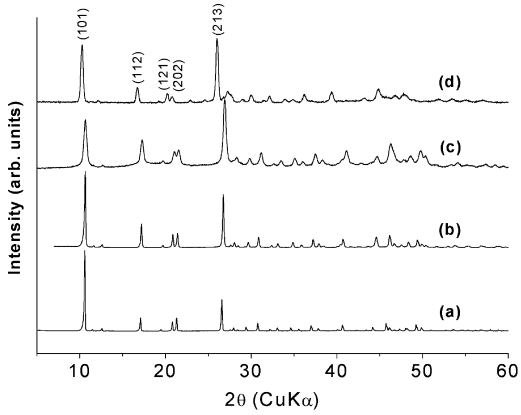

Figure 6. Powder X-ray diffraction patterns of (a) $(Me_4N)_2Fe[Sn_4Se_{10}]$, (b) $(Me_4N)_2Co[Sn_4Se_{10}]$, (c) $(Me_4N)_2Zn[Sn_4Se_{10}]$, and (d) $(Me_4N)_2Mn[Ge_4Te_{10}]$.

are 101.09(3)° (see Figure 4 and Table 4). This large distortion from the ideal T_d symmetry of the transition metal linking cations is common in the isostructural series $(Me_4N)_2M[Ge_4Q_{10}]$ ($M = Mn^{2+}$, Fe^{2+}, Co^{2+}, Zn^{2+}; $Q = S$, Se) and results from binding three adamantane clusters into a ring motif.[39−44]

The excellent agreement between the powder XRD pattern of the bulk solids with the simulated powder pattern from the single crystal data indicates the formation of pure products, see Figure 5. Very similar powder XRD patterns are observed in the case of iron and cobalt indicating the formation of isostructural solids, as shown in Figure 6. When zinc was employed as the linking cation, a disordered phase was formed as judged by the broad Bragg peaks in the corresponding powder XRD pattern. However, crystalline material (see Figure 6) was obtained when Na_4EDTA was used as a complexing agent for Zn^{2+}, presumably by slowing down the kinetics of the self-assembly reaction. The refined lattice parameters of $(Me_4N)_2M[Sn_4Se_{10}]$ ($M = Fe^{2+}$, Co^{2+}, Zn^{2+}) are shown in Table 5. The observed contraction of both *a*- and *c*-lattice constants correlates well with the decrease of the ionic radius of the divalent 3d transition metal cations. The powder XRD pattern of the tellurogermanate analogue $(Me_4N)_2Mn[Ge_4Te_{10}]$ is shown also in Figure 6, and the corresponding lattice constants are in Table 5.

Table 5. Refined Lattice Constants, Color, and Energy Band Gaps of the Microporous $(Me_4N)_2M'[M_4Q_{10}]$ Materials

	tetragonal $I\bar{4}$ lattice constants			
compound	*a* (Å)	*c* (Å)	color	band gap, eV
$(Me_4N)_2Mn[Sn_4Se_{10}]$	9.932(2)	15.374(3)	red	2.06
$(Me_4N)_2Fe[Sn_4Se_{10}]$	9.924(7)	15.356(3)	black	1.27
$(Me_4N)_2Co[Sn_4Se_{10}]$	9.909(7)	15.158(8)	orange	1.93
$(Me_4N)_2Zn[Sn_4Se_{10}]$	9.832(2)	15.082(7)	yellow-orange	2.23
$(Me_4N)_2Mn[Ge_4Te_{10}]$	10.206(6)	15.491(5)	black	0.69

Mössbauer Spectroscopy. ^{57}Fe and ^{119}Sn Mössbauer spectroscopies were used to characterize the Fe and Sn local environment and formal oxidation states in $(Me_4N)_2Fe[Sn_4Se_{10}]$ and $(Me_4N)_2M[Sn_4Se_{10}]$ ($M = Mn^{2+}$, Co^{2+}, Zn^{2+}). The ^{57}Fe Mössbauer spectrum of $(Me_4N)_2Fe[Sn_4Se_{10}]$ at 80 K consists of a doublet with an isomer shift $\delta = 0.64$ mm s^{-1} and a quadrupole splitting ΔE_q of 3.791 mm s^{-1}; see Figure 7. These are consistent with Fe^{2+} in a highly distorted tetrahedral environment of chalcogenide ligands.[52] In the corresponding ^{119}Sn spectrum recorded at 80 K (Figure 8a) the major component (84% area)[53] is a doublet with an isomer shift of $\delta = 1.53$ mm s^{-1} and a small quadrupole splitting ΔE_q of 0.61 mm s^{-1}, typical of tetrahedral Sn^{4+} in chalcogenides.[54] Very similar spectra were obtained for the isostructural solids as shown in Figure 9. The results are consistent with the fact that the structure contains one crystallographic Sn^{4+} tetrahedral site. For comparison, the ^{119}Sn Mössbauer spectrum of the isolated adamantane clusters in $(Me_4N)_4[Sn_4Se_{10}]$ is shown in Figure 8b. The spectrum shows two doublets of almost equal areas (48% and 52%) with identical isomer shift $\delta = 1.51$ mms^{-1} and a quadrupole splitting ΔE_q of 0.82 mm s^{-1} and 0.80 mm s^{-1}, respectively. These results indicate that there are two very similar but crystallographically nonequivalent Sn sites. This is consistent with the isostructural compound $(Et_4N)_4[Sn_4Se_{10}]$ where two crystallographically nonequivalent free $[Sn_4Se_{10}]^{4-}$ anions exist.[49] The presence of one Sn site in the framework compound with a smaller quadrupole

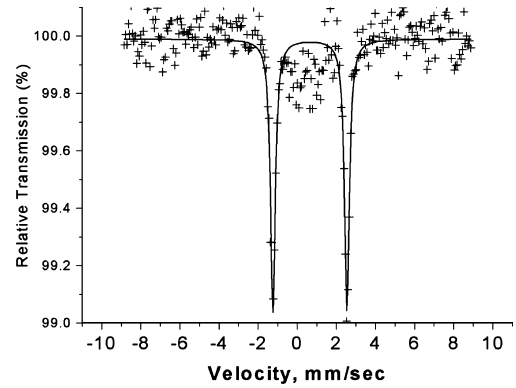

Figure 7. ^{57}Fe Mössbauer spectrum of $(Me_4N)_2Fe[Sn_4Se_{10}]$ recorded at 80 K.

(52) Fatseas, G. A.; Goodenough, J. B. *J. Solid State Chem.* **1980**, *33*, 219–232.

(53) The spectrum contains two minor components: a singlet with a zero isomer shift (7% area) that could be assigned to SnO_2 and a doublet with an isomer shift $\delta = 1.99$ mms^{-1} and a large quadrupole splitting ΔE_q of 2.813 mms^{-1} (9% area).

(54) Lippens, P. E.; Olivier-Fourcade, J.; Jumas, J. C. *Hyperfine Interact.* **2000**, *126*, 137–141.

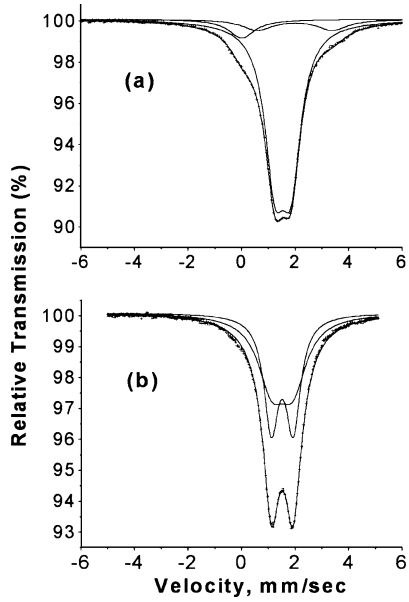

Figure 8. ^{119}Sn Mössbauer spectrum of (a) $(Me_4N)_2Fe[Sn_4Se_{10}]$ and (b) $(Me_4N)_4[Sn_4Se_{10}]$ recorded at 80 K.

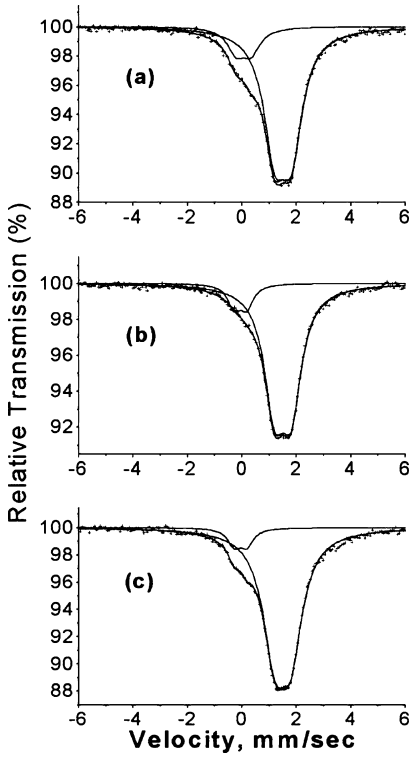

Figure 9. ^{119}Sn Mössbauer spectrum of (a) $(Me_4N)_2Mn[Sn_4Se_{10}]$ (1.49/0.59) and (b) $(Me_4N)_2Co[Sn_4Se_{10}]$ (1.50/0.62) and $(Me_4N)_2Zn[Sn_4Se_{10}]$ (1.51/0.62) recorded at 80 K.

splitting parameter suggests that the $[Sn_4Se_{10}]^{4-}$ clusters become equivalent with a more uniform tetrahedral Sn environment upon their incorporation in the three-dimensional framework.

Infrared and Raman Spectroscopy. Infrared (IR) and Raman spectroscopy was used to examine the metal tin selenide framework in the microporous solids. Figure 10 shows the far-IR spectra of $(Me_4N)_2M[Sn_4Se_{10}]$ and $(Me_4N)_4[Sn_4Se_{10}]$ for comparison. The strong peaks at 230

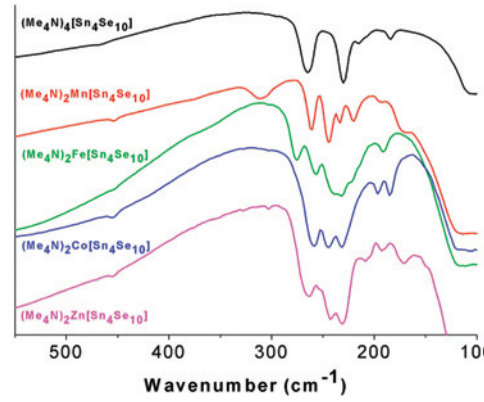

Figure 10. Far-infrared spectra of $(Me_4N)_2M[Sn_4Se_{10}]$ and the precursor salt $(Me_4N)_4[Sn_4Se_{10}]$.

cm^{-1} and 265 cm^{-1} in the spectrum of the free $[Sn_4Se_{10}]^{4-}$ are due to internal modes of the "Sn_4Se_6" core and the terminal Sn−Se stretching modes, respectively. The microporous materials show characteristic peaks in the same range as the free adamantane cluster but are slightly shifted in lower frequencies due to transition metal ligation (see Figure 10 and Table 6). The corresponding Raman spectra are shown in Figure 11. The sharp peak at 180 cm^{-1} in the spectrum of the free $[Sn_4Se_{10}]^{4-}$ is attributed to the total symmetric breathing mode of the "Sn_4Se_6" core and remains almost unaffected in $(Me_4N)_2Mn[Sn_4Se_{10}]$ (183 cm^{-1}). However, the terminal Sn−Se stretching modes which appear at 276, 271, and 126 cm^{-1} for the free cluster $[Sn_4Se_{10}]^{4-}$ are shifted to lower wavenumbers (265 and 107 cm^{-1}) in the framework solid because of the formation of Mn−Se bonds.

Thermal Stability. The thermal stability of the $(Me_4N)_2M[Sn_4Se_{10}]$ materials was investigated with thermogravimetric analysis (TGA). A characteristic TGA curve of $(Me_4N)_2Mn[Sn_4Se_{10}]$ recorded under Ar flow is shown in Figure 12. No appreciable weight loss is observed up to 290 °C consistent with the fact that the solid contains no solvent molecules. This is a remarkably high thermal stability for an organic containing material. A sharp weight loss (17%) occurs between 280 and 330 °C. The product isolated at 340 °C was found to be amorphous. Presumably, the inorganic framework collapses because reactive CH_3^+ species originating from the decomposition of the $(CH_3)_4N^+$ counterions could remove selenium atoms according to the reaction

$$(Me_4N)_2Mn[Sn_4Se_{10}] \rightarrow \text{“}MnSn_4Se_9\text{”} + 2Me_3N + Me_2Se \quad (3)$$

This thermal decomposition pathway has been observed previously in the isostructural metal germanium sulfides[40,42] and selenides[44] and also in their mesostructured analogues.[55] The residual amorphous "$MnSn_4Se_9$" solid is stable up to 470 °C while on further heating a significant weight loss occurs, presumably associated with further removal of Se atoms. The inorganic residue at 600 °C contains crystalline SnSe.

(55) Trikalitis, P. N.; Rangan, K. K.; Kanatzidis, M. G. *J. Am. Chem. Soc.* **2002**, *124*, 2604–2613.
(56) Wang, J.; Zhao, L.; Gong, K. *J. Magn. Magn. Mater.* **2008**, *320*, 1696–1699.

Table 6. Far-Infrared Absorptions (cm^{-1}) for $(Me_4N)_4[Sn_4Se_{10}]$, $(Me_4N)_2Mn[Sn_4Se_{10}]$, $(Me_4N)_2Fe[Sn_4Se_{10}]$, $(Me_4N)_2Co[Sn_4Se_{10}]$, and $(Me_4N)_2Zn[Sn_4Se_{10}]$ Solids

$(Me_4N)_4[Sn_4Se_{10}]$	$(Me_4N)_2Mn[Sn_4Se_{10}]$	$(Me_4N)_2Fe[Sn_4Se_{10}]$	$(Me_4N)_2Co[Sn_4Se_{10}]$	$(Me_4N)_2Zn[Sn_4Se_{10}]$
184 (m)	220 (m, sh)	191 (m, sh)	184 (m, sh)	171 (m,sh)
215 (m)	234 (m, sh)	221 (m)	196 (m, sh)	192 (m)
230 (vs)	244 (vs)	232 (m, sh)	231 (s)	208 (m)
265 (vs)	261 (vs)	240 (m, sh)	245 (s)	231 (s)
		257 (s)	259 (s)	243 (s)
		276 (s)		264 (s)

Magnetism. Magnetic susceptibility measurements performed on polycrystalline samples of $(Me_4N)_2M[Sn_4Se_{10}]$ (M = Mn^{2+}, Fe^{2+}, Co^{2+}) confirm the presence of paramagnetic divalent transition metal cations in tetrahedral coordination. We note that magnetic measurements on $(Me_4N)_2M[Ge_4Q_{10}]$ have not been reported to date. Shown in Figure 13 is the magnetic susceptibility as a function of temperature between 5 and 290 K. The calculated magnetic moments from fitting the linear plot (Curie−Weiss law) of the inverse magnetic susceptibility versus temperature (see inset in Figure 13) are 5.9, 4.4, and 4.4 μ_B for Mn^{2+}, Fe^{2+}, and Co^{2+} containing samples, and the Curie−Weiss constants θ are −2.9, −2.3, and −10.6, respectively. For $(Me_4N)_2Mn[Sn_4Se_{10}]$, the corresponding value correlates very well with the calculated spin-only magnetic moment for tetrahedral $Mn^{2+}(d^5: e^2t_2^3)$ (5.92 μ_B). In the case of iron and cobalt containing solids the observed magnetic moments are somewhat different from the values calculated for tetrahedral $Fe^{2+}(d^6: e^3t_2^3)$ (4.90 μ_B) and $Co^{2+}(d^7: e^4t_2^3)$ (3.88 μ_B), respectively. In a very recent report, theoretical calculations suggested that the $(Me_4N)_2Fe[Ge_4S_{10}]$ should be a half-metallic ferromagnetic compound.[56] It would be very interesting if these results could be confirmed experimentally.

Optical Properties. The optical absorption properties of $(Me_4N)_2M[Sn_4Se_{10}]$ (M = Mn^{2+}, Fe^{2+}, Co^{2+}, Zn^{2+}) and $(Me_4N)_2Mn[Ge_4Te_{10}]$ materials were investigated with solid state diffuse reflectance UV−vis/near IR spectroscopy. All solids possess well-defined, sharp optical absorptions associated with band gap transitions in the energy range 0.7−2.2 eV (see Table 5 and Figure 14). The additional sharp absorption at 1.5 eV (827 nm) in the spectrum of $(Me_4N)_2Co[Sn_4Se_{10}]$ is attributed to d−d electronic transitions associated with the tetrahedral cobalt atom. The high intensity of these transitions arises from the essentially allowed nature of such excitations in tetrahedral complexes. As expected, the observed band gap energies in the isostructural $(Me_4N)_2M[Sn_4Se_{10}]$ series are red-shifted compared to the absorption energy of the molecular precursor compound $(Me_4N)_4[Sn_4Se_{10}]$ (~2.40 eV) because of the formation of

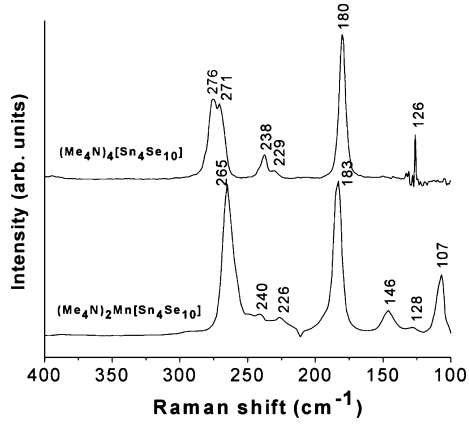

Figure 11. Raman spectra of $(Me_4N)_4[Sn_4Se_{10}]$ and $(Me_4N)_2Mn[Sn_4Se_{10}]$.

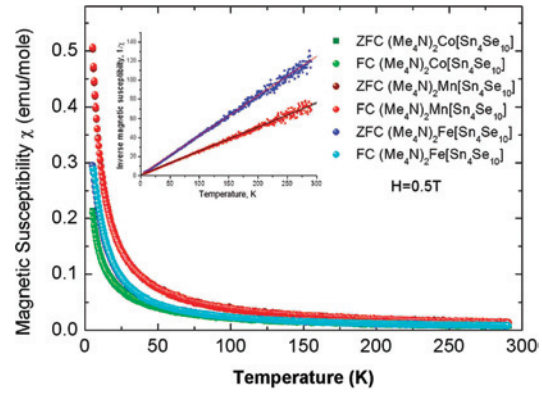

Figure 13. Magnetic susceptibility as a function of temperature for $(Me_4N)_2M[Sn_4Se_{10}]$ (M = Mn^{2+}, Fe^{2+}, Co^{2+}) materials.

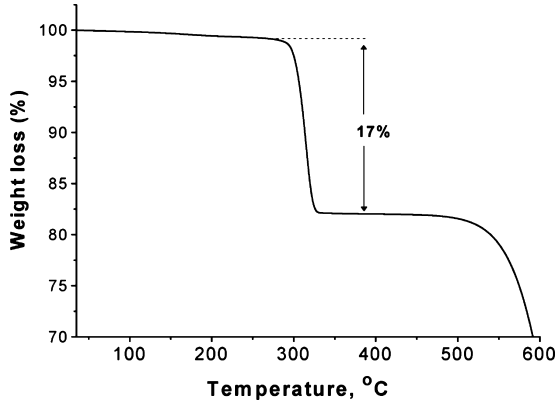

Figure 12. TGA curve of $(Me_4N)_2Mn[Sn_4Se_{10}]$ recorded under Ar flow (heating rate 5 deg/min).

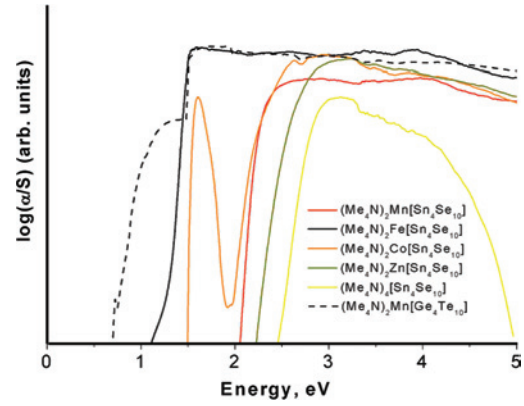

Figure 14. UV−vis electronic absorption spectra of $(Me_4N)_2M[Sn_4Se_{10}]$ and $(Me_4N)_2Mn[Ge_4Te_{10}]$ materials.

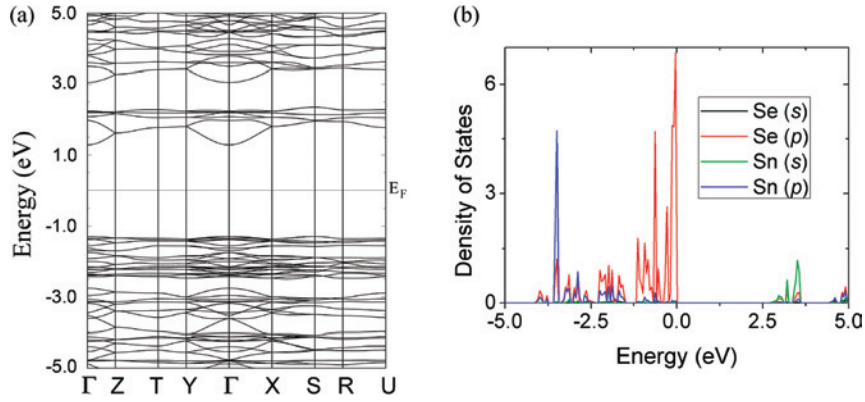

Figure 15. (a) Band structure and (b) the projected density of states for s- and p-orbitals of individual elements (Se and Sn), for hypothetical $Cs_2Zn[Sn_4Se_{10}]$.

extended covalent networks. In the precursor compound, the optical absorption is due to the local intracluster excitations rather than across electron bands.

Interestingly, similar trends and absorption energies were found in the mesostructured $(CP)_{4-2x}M_x[SnSe_4]$ materials[57] (Mn^{2+}: 2.0 eV, Fe^{2+}: 1.4 eV, Zn^{2+}: 2.5 eV) containing the same elements but a different type of selenostannate building units. The results indicate that the elemental composition in these two different classes of open framework solids controls their optical properties. Also notable is the much larger red shift in the band gap energy in going from the selenide $(Me_4N)_2Mn[Sn_4Se_{10}]$ (2.06 eV) to the telluride $(Me_4N)_2Mn[Ge_4Te_{10}]$ (0.69 eV) analogue. The latter is among the lowest band gaps reported in the entire family of open-framework chalcogenides.

Electronic Structure Calculations. Ab-initio density functional calculations with the full-potential linearized augmented plane wave (FLAPW) method[58] were performed to better understand the optical properties of these materials. For simplicity in carrying out these calculations we focused on the Zn analogue $(Me_4N)_2Zn[Sn_4Se_{10}]$ because Zn has a fully occupied d-shell. The partially occupied *d*-orbitals of the transition metal atoms (Mn, Fe, Co) are expected to dominate the band gap region. Furthermore, because the hydrogen coordinates are unknown, a hypothetical model was created by replacing the organic cation $(CH_3)_4N^+$ with Cs^+, that is, $Cs_2Zn[Sn_4Se_{10}]$. This is based on the expectation that an organic cation such as tetramethyl ammonium $(CH_3)_4N^+$ does not play any significant role in the electronic structure of the framework other than simply balancing charge.

The electronic structures were calculated with the fully first-principles screened-exchange local density functional approximation (sX-LDA) scheme[59,60] within the highly precise FLAPW method. The sX-LDA method has been successfully applied to yield or predict excited electronic states such as band gaps and band dispersion due to its better long-range description of the exchange-correlation hole compared to the local density approximation (LDA).

The electronic structure calculations by the sX-LDA calculated an indirect band gap of 2.57 eV as shown in Figure 15a, which is close to the experimental band gap, 2.23 eV. The valence band maximum (VBM) occurs at the S-point in Figure 15a while the conduction band minimum (CBM) is located at the Γ-point, which leads to an indirect band gap. However, the energy difference between the S-point and Γ-point of the valence band top is approximately only 0.012 eV, which is responsible for the sharp absorption coefficient measurement in the band gap region. Therefore, we conclude that the experimentally measured E_g is the result of direct transitions.

The angular-momentum-resolved density of states (DOS) for Se and Sn in Figure 15b shows the s−p hybridization with ionic character. The valence band minimum is dominated by Se p-orbitals while the conduction band minimum shows a relatively stronger contribution from the Sn s-orbitals. Hence the optical transition observed experimentally in $(Me_4N)_2Zn[Sn_4Se_{10}]$ occurs mainly between Se p-orbitals and Sn s-orbitals. The calculations also suggest that the contribution of Cs and Zn s-orbitals is negligible especially near the band gap region, and so they are not included in Figure 15b. This supports the idea of the replacement ($(CH_3)_4N$) with Cs in the hypothetical model employed here. The band gap features will be very different in the other transition metal analogues (Mn, Fe, and Co). In the Zn analogue $(Me_4N)_2Zn[Sn_4Se_{10}]$, the Zn d-orbitals are located mainly at about −11 eV below the Fermi level E_F because of their fully occupied d-shell. On the other hand, other transition metal analogues are expected to have d-orbital levels much closer to E_F and strong p−d hybridization. Thus, their d-orbitals dominate the optical transitions near the band gap region, as shown in the experimental measurements. From these findings, we can conclude that the substantially narrower gap of the MGe_4Te_{10} composition arises from the higher energy of the Te p-orbitals which comprise the top of the valence band.

(57) Trikalitis, P. N.; Rangan, K. K.; Bakas, T.; Kanatzidis, M. G. *Nature* **2001**, *410*, 671–675.
(58) Wimmer, E.; Krakauer, H.; Weinert, M.; Freeman, A. J. *Phys. Rev. B* **1981**, *24*, 864–875.
(59) Asahi, R.; Mannstadt, W.; Freeman, A. J. *Phys. Rev. B* **1999**, *59*, 7486–7492.
(60) Bylander, D. M.; Kleinman, L. *Phys. Rev. B* **1990**, *41*, 7868–7871.
(61) WinPLOTR: a Windows tool for powder diffraction patterns analysis. *Materials Science Forum, Proceedings of the Seventh European Powder Diffraction Conference (EPDIC 7), Barcelona Spain, May 20–23, 2000*; Delhez, R., Mittenmeijer, E. J., Eds.; 2001, pp 118−123, Trans Tech Publications, Switzerland (http://wwwold.ill.fr/dif/Soft/fp/).

Conclusions

A large set of adamantane clusters $[Sn_4Q_{10}]^{4-}$ (Q = S, Se, Te) can be synthesized on a multigram scale using a simple, fast, and inexpensive method. This now allows their convenient use as building blocks for the assembly of a wide variety of framework compounds with tunable properties. One example is the family of solids with the chemical formula $(Me_4N)_2M[Sn_4Se_{10}]$ ($M = Mn^{2+}$, Fe^{2+} Co^{2+}, Zn^{2+}) described here. These materials represent the heavier analogues of the microporous $(Me_4N)_2M[Ge_4Q_{10}]$ (Q = S, Se) solids and exhibit lower band gap energies found between 1.27 and 2.23 eV. This is in the desirable region for many optical applications including the harvesting of solar energy. We also succeeded in synthesizing the first telluride analogue $(Me_4N)_2Mn[Ge_4Te_{10}]$ which exhibits the narrowest band gap of this family of compounds at 0.69 eV. Currently, we focus on the development of suitable methodologies to access the available pore space in these materials.

Acknowledgment. The research was supported financially by the European Union (75%) and the Greek Government (25%) through the program PENED-2003 code number 03ED450 and from the INTERREG IIIA Greece-Cyprus (K2301.004). Financial support from the National Science Foundation (NSF) (DMR-0801855) and through its MRSEC program (DMR-0520513) at the Materials Research Center of Northwestern University is gratefully acknowledged.

Supporting Information Available: Crystallographic information in CIF format. This material is available free of charge via the Internet at http://pubs.acs.org.

IC801762H